ChemComm

ROYAL SOCIETY OF CHEMISTRY

COMMUNICATION

View Article Online
View Journal | View Issue

Cite this: *Chem. Commun.*, 2020, **56**, 6826

Received 2nd April 2020,
Accepted 6th May 2020

DOI: 10.1039/d0cc02382e

rsc.li/chemcomm

A large axial magnetic anisotropy in trigonal bipyramidal Fe(II)†

Moya A. Hay, [a] Arup Sarkar, [b] Gavin A. Craig, ‡[a] Katie E. R. Marriott,[a] Claire Wilson, [a] Gopalan Rajaraman *[b] and Mark Murrie *[a]

The first trigonal bipyramidal Fe(II) complex to display slow relaxation of magnetisation has been isolated, with this behaviour found to arise through a combination of a large magnetic anisotropy (D = −27.5 cm^{-1}) and a pseudo-D_{3h} symmetry at the Fe(II) centre, as investigated through *ab initio* and magnetic studies.

The continuing demand for the miniaturisation of technology to maximise data storage density drives research into molecular magnetic materials. One class of such materials are single-molecule magnets (SMMs), which show slow relaxation of the magnetisation.[1,2] Engineering SMM properties to maximise the retention of magnetisation has led to molecular magnetic hysteresis up to 80 K.[3–5] Initially increasing the spin ground state S was the focus, however maximising the axial magnetic anisotropy has become more extensively investigated.[6,7] For example in cases where an uneven number of electrons reside in degenerate orbitals, as is the case with Ni(II) [or Fe(II)] in a trigonal bipyramidal (TBP) coordination environment, if antagonistic Jahn–Teller distortions can be minimised through the judicious choice of ligands a 'giant' magnetic anisotropy can be induced.[8,9] This strategy was used successfully for the TBP Ni(II) complex $[NiCl_3(MDABCO)_2][ClO_4]$ ($[MDABCO]^+$ = 1-methyl-4-aza-1-azoniabicyclo[2.2.2]octanium cation).[10–12] In light of the potential to induce a large magnetic anisotropy in TBP Fe(II) using this strategy, and the interest in the magnetic properties of monometallic Fe(II) complexes,[13–17] we report the synthesis of $[FeCl_3(MDABCO)_2][ClO_4]$ (**1**). In conjunction with *ab initio* calculations, experimental investigations of the magnetic properties of **1** have confirmed it to be the first example of a TBP Fe(II) coordination complex to display slow relaxation of the magnetisation.

For the synthesis of **1** see Section S1, ESI.† $[FeCl_3(MDABCO)_2][ClO_4]$ (**1**) is isomorphous with the previously reported Ni(II) analogue possessing two axial $[MDABCO]^+$ ligands and three equatorial chloride ligands, and crystallises in the orthorhombic $Pca2_1$ space group (Fig. 1).[10] In the unit cell there are four different orientations of the $[Fe(MDABCO)_2Cl_3]^+$ cation that result in intermolecular Fe···Fe distances between 8.4996(2) and 13.185(3) Å. Continuous shape measures (CShMs) were used to quantify the distortion around the Fe(II) centre, with a value of 0 assigned when the experimentally obtained atomic positions match the ideal TBP coordination environment.[18–20] The CShM value of 0.057 shows that there is only a very small deviation from the ideal TBP environment.

CASSCF/NEVPT2 calculations have been performed on **1** to probe the origin of the magnetic anisotropy, as this method is found to yield good numerical estimates of zero-field splitting (ZFS) parameters for transition metal complexes.[21,22] These calculations give an axial ZFS (D) of −27.5 cm^{-1} with a minimal transverse, or rhombic, E/D value of 0.02. This is in sharp contrast to a recently reported Fe(II) trigonal bipyramidal

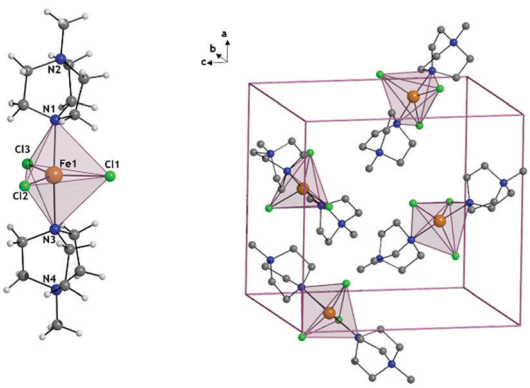

Fig. 1 The structure of $\mathbf{1}^+$ cation (left) and the unit cell (right) where anions and hydrogen atoms have been omitted for clarity.

[a] *School of Chemistry, University of Glasgow, University Avenue, Glasgow, G12 8QQ, UK. E-mail: mark.murrie@glasgow.ac.uk*
[b] *Department of Chemistry, Institute of Technology Bombay, Powai, Mumbai, Maharashtra, 400 076, India. E-mail: rajaraman@chem.iitb.ac.in*

† Electronic supplementary information (ESI) available: Synthetic procedures, crystallographic data, powder X-ray diffraction (PXRD) patterns, and additional magnetic measurements. CCDC 1992135. For ESI and crystallographic data in CIF or other electronic format see DOI: 10.1039/d0cc02382e

‡ Present address: Department of Pure and Applied Chemistry, University of Strathclyde, Glasgow, UK.

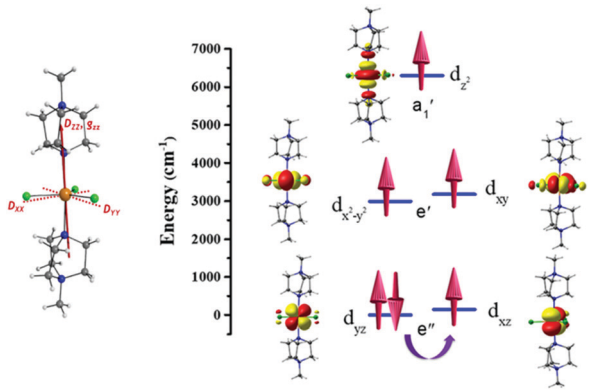

Fig. 2 D and g_{zz} tensor directions (left), NEVPT2-LFT computed d-orbital energies in **1** (right).

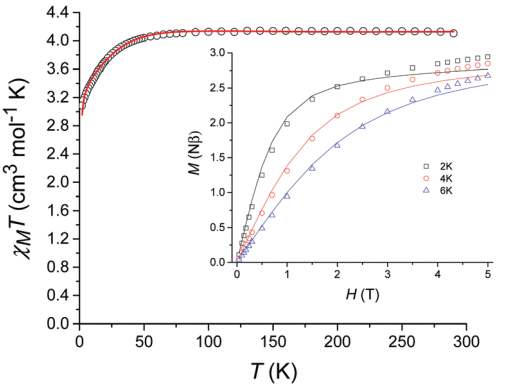

Fig. 3 Temperature dependence of $\chi_M T$ for **1** from 290 K to 2 K in a dc field of 1000 Oe (magnetization *vs.* field shown inset). The solid lines correspond to the fit (see text for details).

complex where a small positive D value resulted, which can be attributed to the differences in geometric distortion (CShM value of 0.057 for **1** *vs.* 1.050 for $[Fe(MST)(OH_2)]^-$ where $[H_3MST]$ = *N*,*N*′,*N*″-[2,2′,2″-nitrilotris-(ethane-2,1-diyl)]tris(2,4,6-trimethylbenzene-sulfonamide)).[13] The computed D_{zz} or g_{zz} anisotropy axes for **1** lie very close to the N–Fe–N axis of the complex (see Fig. 2). The large negative D value is primarily due to mixing with the 1st excited state ($^5E_y''$), which corresponds to the same M_L level $d_{yz} \rightarrow d_{xz}$ electronic transition (see Table S4, ESI† and Fig. 2). In ideal D_{3h} symmetry the $^5E_x''$ and $^5E_y''$ states are degenerate, but a small Jahn–Teller distortion results in the 1st excited state in **1** lying 137 cm^{-1} above the ground state (see Table S4, ESI†). While this 1st excited state provides the largest contribution to the overall D value, mixing of other quintet excited states also provide small (positive) contributions to D (see Table S4, ESI†). As was observed with the Ni(II) analogue, the significant steric bulk of the axial ligands prevents the Jahn–Teller distortion modes. This retains a high-order pseudo-D_{3h} symmetry around Fe(II) centre, which is reflected in the negligible E/D value.[11,12] The spin–orbit coupling analysis reveals a very small tunnel splitting (0.08 cm^{-1}) for the $M_S = \pm 2$ levels but the reduced weightage in the spin–orbit states ($|\pm 2\rangle$) suggests strong ground state quantum tunnelling (see Table S5, ESI†), which rationalises the observation of field-induced (rather than zero field) slow magnetic relaxation (*vide infra*), despite the favourable D and E/D parameters.

The variable-temperature magnetic susceptibility data for **1** were collected between 290 K and 2 K under an applied direct-current (dc) field of 1000 Oe (Fig. 3). At 290 K, the $\chi_M T$ value of 4.10 $cm^3\ mol^{-1}$ K is substantially higher than that expected for a spin-only model ($S = 2$, $g = 2$, $\chi_M T = 3.0\ cm^3\ mol^{-1}$ K) indicating a significant residual orbital moment. $\chi_M T$ remains almost constant until approximately 50 K after which a sharp decrease is observed, reaching a minimum value of 3.08 $cm^3\ mol^{-1}$ K at 2 K. The magnetisation measurements (M *vs.* H) were carried out between 0 and 5 T at 2, 4 and 6 K (Fig. 3 inset) and in each case did not reach saturation.

$$\hat{H} = D\hat{S}_z^2 + E\left(\hat{S}_x^2 - \hat{S}_y^2\right) + \mu_B \vec{B} \cdot \overleftrightarrow{g} \cdot \hat{S} \qquad (1)$$

The $\chi_M T$ *vs.* T and M *vs.* H data were fitted simultaneously using the program *Phi*[23] using the Hamiltonian presented in eqn (1). Some parameters were fixed based on the results obtained from the *ab initio* calculations (*vide supra*): the axial and rhombic ZFS parameters, D and E, were fixed at values of −27.5 cm^{-1} and 0.58 cm^{-1}, respectively as well as $g_x = 1.90$ and $g_y = 1.98$. The g_z value however was fixed at 2.61 considering the local minimum in the residual determined *via* a survey of the $\chi_M T$ *vs.* T data, although it should be noted that this is close to the *ab initio* determined g_z value of 2.53. TIP and zJ terms were determined from the fit (further details can be found in the ESI† along with additional fits and survey plots (see Fig. S2 and S3)).

Initial investigations of the dynamic susceptibility were carried out as a function of field with H_{dc} ranging between 0 and 5000 Oe at a fixed temperature of 2 K (see Fig. 4 and Fig. S4, ESI†).

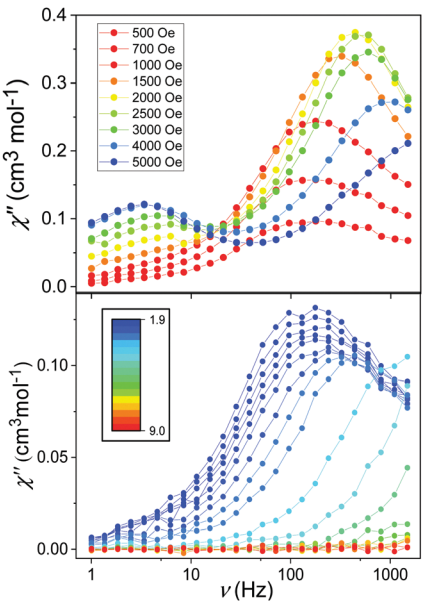

Fig. 4 Frequency-dependence of the χ'' response in H_{dc} ranging between 500 and 5000 Oe at 2 K (upper) and in H_{dc} = 600 Oe between 1.9 and 9 K (lower).

No out-of-phase ac χ'' response was observed in zero applied dc field, as is common for monometallic 3d complexes where spin-phonon relaxation and quantum tunnelling of magnetisation (QTM) can be particularly efficient,[24–26] but on applying dc fields of above 500 Oe a frequency dependence was observed.[8] At $H_{dc} \leq 1500$ Oe, a single high frequency (HF) relaxation pathway is apparent. On increasing H_{dc} above 1500 Oe, a second low frequency (LF) relaxation path emerges (see Fig. 4). The co-existence of two relaxation regimes has been previously attributed to relaxation originating from the individual complexes for the HF pathway, with the LF pathway arising due to intermolecular interactions.[27–31] This leads to a difference in behaviour as a function of temperature, with the signal arising from the HF pathway exhibiting a temperature dependence and that from the LF path remaining temperature independent. We therefore chose to investigate the variable temperature ac susceptibility at two fields; 600 Oe where only the HF relaxation mode is observable, and 2500 Oe where the LF pathway emerges, and the HF mode is under an optimal field (see Fig. S6 and S7, ESI†). Under an H_{dc} of 600 Oe clear maxima are observed in the out-of-phase signal, which move beyond the frequency limit of the SQUID above 3.5 K (Fig. 4). When probed under an H_{dc} up to 2500 Oe, the HF signal is now maximised and once again moves out of the frequency range above 3.5 K (Fig. S7, ESI†). Additionally, the LF mode is now observable and exhibits no obvious temperature dependence. This is more apparent on consideration of the respective Arrhenius plots ($\ln\tau$ *vs.* $1/T$) shown in Fig. 5 constructed using the relaxation rates, τ, extracted from the fit of the Argand diagrams (Fig. S8, ESI†). At 600 Oe the HF relaxation channel shows a crossover to temperature independent relaxation when tending to lower temperatures. At 2500 Oe, a larger contribution from temperature independent relaxation processes is evident for the HF relaxation channel. As expected, the τ values for the LF pathway show no clear temperature dependence.

Given that the HF relaxation regime is that arising from the isolated Fe(II) complex, and that the strongest temperature dependence of τ is observed above 3.5 K, a crude estimate of the barrier to spin reversal using the corresponding relaxation rates was made in accordance with the Arrhenius law given by the first term in eqn (2) (see Fig. S9, ESI†).

For the data collected at 600 Oe, the gradient of the straight-line approximation, corresponding to $\Delta E/k_B$, was estimated to be 52.9 ($\pm$4.6) K (36.7 ($\pm$3.2) cm^{-1}), which is substantially lower than that estimated based on the D parameter obtained from the *ab initio* calculations ($4|D| = 110$ cm^{-1}). At 2500 Oe $\Delta E/k_B$ is even lower at 13.8 ($\pm$0.3) K (9.6 ($\pm$0.2) cm^{-1}). This suggests that other relaxation processes short-cut the thermal energy barrier, and discounts a model including the Orbach term as this process must occur *via* 'real' states (*e.g.* $\sim 3|D|$ (82.5 cm^{-1}) for $M_S \pm 2$ and ± 1). The fit was then reconsidered to account for spin–lattice direct processes

$$\tau^{-1} = \tau_0^{-1} \exp\left(-\frac{\Delta E}{k_B T}\right) + AH^2T + CT^n + \frac{B_1}{1 + B_2H^2} \qquad (2)$$

and Raman processes, given by the second and third terms in eqn (2), respectively, as well as a QTM contribution denoted by the fourth term in eqn (2) (see Fig. S11, ESI†).[32]

To avoid over-parameterisation, the field dependence of the relaxation rate was initially fitted using the field-dependent processes (see Fig. S10, ESI†). This allowed us to extract parameters relating to both direct relaxation and QTM (A, B_1 and B_2) giving A = 182.35 ($\pm$0.05) $\times$ 10^2 s^{-1} kOe^{-2} K^{-1}, B_1 = 109.60 ($\pm$0.04) $\times$ 10 s^{-1} and B_2 = 355.57 ($\pm$2.56) $\times$ 10^{-2} kOe^{-2}. Once obtained, these parameters were fixed in the fits of the temperature dependence of the relaxation rates at both 600 Oe and 2500 Oe. For data collected at H_{dc} = 600 Oe, the fit fixing A, B_1 and B_2 and n = 7 for an integer spin ion is shown in Fig. S11 (ESI†) where C = 5.64 ($\pm$0.06) s^{-1} K^{-n}. The fit can be improved by including an Orbach term but as discussed earlier it is not appropriate to include this term based on the estimated energy gap between 'real' states. For relaxation rates obtained under 2500 Oe the data could be fitted by fixing A but it was not possible to do this for the QTM terms B_1 and B_2. The Raman parameters obtained were C = 1.31 ($\pm$0.01) s^{-1} K^{-n}, n = 6.39 ($\pm$0.01). The general QTM term obtained from the fit (1.34 ($\pm$0.01) $\times$ 10^3 s^{-1}) was close to that obtained based on the field dependent relaxation rates ($(B_1/1 + B_2H^2) \sim 9 \times 10^2$ s^{-1}).

[FeCl$_3$(MDABCO)$_2$][ClO$_4$] (**1**) is the first monometallic trigonal bipyramidal Fe(II) complex to show slow relaxation of the magnetisation. Rigorous control of the coordination environment produces a large axial magnetic anisotropy as confirmed by dc magnetic measurements and supported by *ab initio* calculations. Due to the rarity of slow magnetic relaxation in TBP Fe(II), even under an applied dc field, we stress the importance of minimising the geometric distortion in order to generate a large axial magnetic anisotropy while also minimising the rhombic magnetic anisotropy.

The UK Engineering and Physical Sciences Research Council are thanked for financial support (grant ref. EP/J018147/1). GR thanks SERB (CRG/2018/000430) and UGC-UKEIRI (Grant number 184-4/2018(IC)) for funding. AS thanks NPSF CDAC Pune for providing access to the supercomputing facility and CSIR for an SRF fellowship.

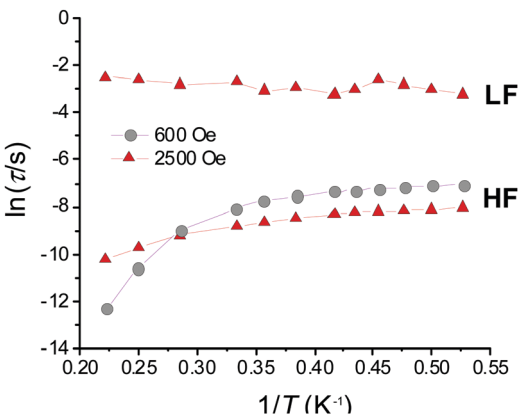

Fig. 5 Arrhenius plot of the high-frequency (HF) and low-frequency (LF) modes at 600 and 2500 Oe constructed from the extracted values of τ obtained from the fit of the Argand diagrams for data between 1.9–4.5 K. Solid lines are a guide for the eye only.

Conflicts of interest

There are no conflicts to declare.

Notes and references

1 C. Benelli and D. Gatteschi, *Introduction to Molecular Magnetism: From Transition Metals to Lanthanides*, Wiley-VCH, Florence, 1st edn, 2015.
2 R. Sessoli, D. Gatteschi, A. Caneschi and M. A. Novak, *Nature*, 1993, **365**, 141–143.
3 C. A. P. Goodwin, F. Ortu, D. Reta, N. F. Chilton and D. P. Mills, *Nature*, 2017, **548**, 439–442.
4 F.-S. Guo, B. M. Day, Y.-C. Chen, M.-L. Tong, A. Mansikkamäki and R. A. Layfield, *Angew. Chem., Int. Ed.*, 2017, **56**, 11445–11449.
5 F.-S. Guo, B. M. Day, Y.-C. Chen, M.-L. Tong, A. Mansikkamäki and R. A. Layfield, *Science*, 2018, **362**, 1400–1403.
6 N. Ishikawa, M. Sugita, T. Ishikawa, S. Y. Koshihara and Y. Kaizu, *J. Am. Chem. Soc.*, 2003, **125**, 8694–8695.
7 W. H. Harman, T. D. Harris, D. E. Freedman, H. Fong, A. Chang, J. D. Rinehart, A. Ozarowski, M. T. Sougrati, F. Grandjean, G. J. Long, J. R. Long and C. J. Chang, *J. Am. Chem. Soc.*, 2010, **132**, 18115–18126.
8 G. A. Craig and M. Murrie, *Chem. Soc. Rev.*, 2015, **44**, 2135–2147.
9 S. Gomez-Coca, E. Cremades, N. Aliaga-Alcalde and E. Ruiz, *J. Am. Chem. Soc.*, 2013, **135**, 7010–7018.
10 K. E. R. Marriott, L. Bhaskaran, C. Wilson, M. Medarde, S. T. Ochsenbein, S. Hill and M. Murrie, *Chem. Sci.*, 2015, **6**, 6823–6828.
11 G. A. Craig, A. Sarkar, C. H. Woodall, M. A. Hay, K. E. R. Marriott, K. V. Kamenev, S. A. Moggach, E. K. Brechin, S. Parsons, G. Rajaraman and M. Murrie, *Chem. Sci.*, 2018, **9**, 1551–1559.
12 M. Gruden-Pavlović, M. Perić, M. Zlatar and P. García-Fernández, *Chem. Sci.*, 2014, **5**, 1453–1462.
13 K. A. Schulte, K. R. Vignesh and K. R. Dunbar, *Chem. Sci.*, 2018, **9**, 9018–9026.
14 X. Liu, J. Zhou, X. Bao, Z. Yan, G. Peng, M. Rouzières, C. Mathonière, J.-L. Liu and R. Clérac, *Inorg. Chem.*, 2017, **56**, 12148–12157.
15 C. Baldé, N. Paradis, C. Desplanches and G. Chastanet, *Eur. J. Inorg. Chem.*, 2018, 14741–14750.
16 P. Stock, E. Deck, S. Hohnstein, J. Korzekwa, K. Meyer, F. W. Heinemann, F. Breher and G. Hörner, *Inorg. Chem.*, 2016, **55**, 5254–5265.
17 A. Urtizberea and O. Roubeau, *Chem. Sci.*, 2017, **8**, 2290–2295.
18 M. Pinsky and D. Avnir, *Inorg. Chem.*, 1998, **37**, 5575–5582.
19 D. Casanova, J. Cirera, M. Llunell, P. Alemany, D. Avnir and S. Alvarez, *J. Am. Chem. Soc.*, 2004, **126**, 1755–1763.
20 S. Alvarez, *Chem. Rev.*, 2015, **115**, 13447–13483.
21 A. Sarkar, G. Velmurugan, T. Rajeshkumar and G. Rajaraman, *Dalton Trans.*, 2018, **47**, 9980–9984.
22 T. Gupta and G. Rajaraman, *Chem. Commun.*, 2016, **52**, 8972–9008.
23 A. Soncini, K. S. Murray, N. F. Chilton, R. P. Anderson and L. D. Turner, *J. Comput. Chem.*, 2013, **34**, 1164–1175.
24 A. Lunghi, F. Totti, S. Sanvito and R. Sessoli, *Chem. Sci.*, 2017, **8**, 6051–6059.
25 D. Gatteschi and R. Sessoli, *Angew. Chem., Int. Ed.*, 2003, **42**, 268–297.
26 A. Lunghi, F. Totti, R. Sessoli and S. Sanvito, *Nat. Commun.*, 2017, **8**, 14620.
27 J. Miklovic, D. Valigura, R. Boča and J. Titiš, *Dalton Trans.*, 2015, **44**, 12484–12487.
28 D. Valigura, C. Rajnak, J. Moncol, J. Titiš and R. Boča, *Dalton Trans.*, 2017, **46**, 10950–10956.
29 R. Boča, C. Rajnák, J. Titiš and D. Valigura, *Inorg. Chem.*, 2017, **56**, 1478–1482.
30 A. Świtlicka, B. Machura, M. Penkala, A. Bieńko, D. C. Bieńko, J. Titiš, C. Rajnák, R. Boča, A. Ozarowski and M. Ozerov, *Inorg. Chem.*, 2018, **57**, 12740–12755.
31 C. Rajnák, F. Varga, J. Titiš, J. Moncol and R. Boča, *Inorg. Chem.*, 2018, **57**, 4352–4358.
32 K. Shrivastava, *Phys. Status Solidi B*, 1983, **117**, 437–458.